An Interlaboratory Comparison of Sizing and Counting of Subvisible Particles Mimicking Protein Aggregates

DEAN C. RIPPLE,[1] CHRISTOPHER B. MONTGOMERY,[1] ZHISHANG HU[2]

[1]Biomolecular Measurement Division, National Institute of Standards and Technology, Gaithersburg, Maryland
[2]Center for Computational and Systems Biology, Institute of Biophysics, Chinese Academy of Sciences, Beijing, China

Received 2 October 2014; revised 30 October 2014; accepted 3 November 2014

Published online 24 November 2014 in Wiley Online Library (wileyonlinelibrary.com). DOI 10.1002/jps.24287

ABSTRACT: Accurate counting and sizing of protein particles has been limited by discrepancies of counts obtained by different methods. To understand the bias and repeatability of techniques in common use in the biopharmaceutical community, the National Institute of Standards and Technology has conducted an interlaboratory comparison for sizing and counting subvisible particles from 1 to 25 μm. Twenty-three laboratories from industry, government, and academic institutions participated. The circulated samples consisted of a polydisperse suspension of abraded ethylene tetrafluoroethylene particles, which closely mimic the optical contrast and morphology of protein particles. For restricted data sets, agreement between data sets was reasonably good: relative standard deviations (RSDs) of approximately 25% for light obscuration counts with lower diameter limits from 1 to 5 μm, and approximately 30% for flow imaging with specified manufacturer and instrument setting. RSDs of the reported counts for unrestricted data sets were approximately 50% for both light obscuration and flow imaging. Differences between instrument manufacturers were not statistically significant for light obscuration but were significant for flow imaging. We also report a method for accounting for differences in the reported diameter for flow imaging and electrical sensing zone techniques; the method worked well for diameters greater than 15 μm. © 2014 Wiley Periodicals, Inc. and the American Pharmacists Association J Pharm Sci 104:666–677, 2015

Keywords: image analysis; imaging methods; light scattering; microparticles; particle size; physical characterization

INTRODUCTION

Protein particles, consisting of aggregated protein and possibly a nonprotein nucleating core, can form in biopharmaceutical drugs.[1,2] Stresses that can lead to the formation of protein particles include changes in chemical environment, exposure to interfaces, agitation, elevation of temperature, or the introduction of nonprotein particles.[3–7] Counting and characterizing these particles is necessary to assure the quality of these drugs. Although the size of aggregated proteins may vary from 10s of nanometers to 100s of micrometers, the most sensitive analytical techniques cover the approximate range from 1 to 100 μm.[3,8]

In contrast to possible nonprotein impurities (e.g., glass chips, stainless steel particles, and fibers) protein particles have low optical contrast (equivalent to a small refractive index difference from the matrix fluid) and are subject to dynamic changes in size and concentration as particles are formed or dissolve back into solution.[3,9,10] Industry has made great strides in adopting new technologies to count protein particles routinely down to sizes of approximately 2 μm, but particle counts obtained with different types of instruments often differ by as much as a factor of 10.[11,12] Particle counting instruments are commonly calibrated using polystyrene latex (PSL) beads, which have high optical contrast and spherical shape; the observed count discrepancies indicate that instrument calibrations with PSL beads do not suffice to standardize instrument response to protein particles.

Comparison of analytical measurements of particle size and count has been hampered by the instability of the protein particles themselves, which can aggregate further on shipping or revert back to smaller aggregates or monomer protein molecules. As an alternate path to producing a suitable reference material, the National Institute of Standards and Technology (NIST) is developing a reference material comprising irregular particles of a low-refractive index fluoropolymer, ethylene tetrafluoroethylene (ETFE). The morphology and optical contrast of this material closely resembles that of typical protein particles.

As an initial step in implementing this reference material and to assess the level of agreement among different laboratories, NIST has conducted an interlaboratory comparison for sizing and counting subvisible particles from 1 to 25 μm, using a polydisperse polymer suspension that closely mimics actual protein particles. As listed in Table 1, a total of 23 laboratories participated, including 15 from biopharmaceutical manufacturers, one from biomedical device manufacturers, two from instrumentation manufacturers, three from government laboratories, and two from academic laboratories.

This paper describes the design, production, and characterization of the particles (section *Materials and Methods*); gives an overview of the bias between different counting methods (section *Results and Discussion*); and then discusses results for the four methods[8,13] used by participants: flow imaging,[12] light obscuration, electrical sensing zone (ESZ),[14,15] and resonant mass measurement (RMM)[16] (sections *Overview and Identification of Outliers to Resonant Mass Measurement*). Sections

Correspondence to: Dean C. Ripple (Telephone: +301-975-4801; Fax: +301-548-0206; E-mail: dean.ripple@nist.gov)

This article contains supplementary material available from the authors upon request or via the Internet at http://wileylibrary.com.

Journal of Pharmaceutical Sciences, Vol. 104, 666–677 (2015)

Table 1. List of Laboratories That Participated in the Study

Amgen, Inc., Formulation and Analytical Sciences, Thousand Oaks, California
BD Medical, Pharmaceutical Systems, Pharmaceutical technology/R&D, Pont de Claix, France
Biogen Idec, QC Analytical Technology, Research Triangle Park, North Carolina
Bristol Myers Squibb, Biologics Analytical Development and Testing, Pennington, New Jersey
Boehringer Ingelheim Pharma GmbH and Company KG, Biopharmaceuticals, Biberach an der Riss, Germany
Coriolis Pharma, Martinsried, Germany
Eli Lilly and Company, Biopharmaceutical Research and Development, Indianapolis, Indiana
F. Hoffmann-La Roche Ltd, Pharma Technical Development Europe (Biologics), Basel, Switzerland
Food and Drug Administration,[a] Laboratory of Plasma Derivatives, Center for Biologics Evaluation and Research, Bethesda, Maryland
Fluid Imaging Technologies, Yarmouth, Maine
Genentech, Inc., Roche Group, Late Stage Pharmaceutical and Processing Development, South San Francisco, California
Hach Company, Grants Pass, Oregon
GlaxoSmithKline R&D, Biopharm Product Sciences (BPS), King of Prussia, Pennsylvania
GlaxoSmithKline (formerly Human Genome Sciences), Gaithersburg, Maryland
Health Canada, Centre for Biologics Evaluation, Biologics and Genetic Therapies Directorate, Ottawa, Canada
Janssen R&D, Schaffhausen, Switzerland
MedImmune, Formulation Sciences Department, Gaithersburg, Maryland
National Institute of Standards and Technology, Bioprocess Measurements Group, Gaithersburg, Maryland
Novartis Pharma AG, Biologics Process R&D, Basel, Switzerland
Pfizer, Inc., Biotherapeutics Pharmaceutical Sciences, Chesterfield, Missouri
Sandoz Biopharmaceuticals, Pharmaceutical and Device Development, Drug Product Analytics, Sandoz GmbH, Langkampfen, Austria
University of Kansas, Department of Pharmaceutical Chemistry, Macromolecule and Vaccine Stabilization Center, Lawrence, Kansas
University of Leiden, Leiden/Amsterdam Center for Drug Research, Department of Drug Delivery Technology, Gorlaeus Laboratories, Leiden, The Netherlands

[a] Although US FDA laboratory participated in the scientific study and/ or discussion, please note that FDA does not recommend, endorse, or recognize this standard development and further, the content of this communication represents the authors' views and does not bind or obligate FDA.

Particle Morphology and *Resonant Mass Measurement* also describe an initial attempt to adjust the reported diameter of ESZ instruments to be equivalent to the diameter reported by flow imaging instruments.

The results give a snapshot of the level of agreement between different laboratories for the particle counting methods in common use today in the biopharmaceutical industry. As expected from published results on protein particles, particle counts differed significantly depending on the counting method. For each specific method, statistically significant deviations were observed primarily because of differences in instrument response. There were also several outliers (~10% of the reported data) likely related to insufficient resuspension of the ETFE particles and contamination of the ETFE particles by debris from vial-thread abrasion. Surprisingly, data obtained by light obscuration agreed well for small diameter particles [relative standard deviation (RSD) of <26% for lower diameter limits from 1 to 5 μm], but the level of agreement was significantly worse for large particles. For flow imaging, there were statistically significant differences between data sets acquired on different instrument models, resulting in a large variability of counts (RSD values of 33%–61% for all flow imaging data). For specified instrument settings and models, the variability was reduced, with RSD values of 13%–49% over the full size range of the comparison. ESZ instruments gave anomalously high counts for the lowest diameter limits.

MATERIALS AND METHODS

Preparation of the Particle Suspension

The samples circulated for testing consisted of a polydisperse suspension of particles created from the polymer ETFE. ETFE is attractive because it has low refractive index[17] (≈1.40, similar to that of protein films adsorbed on surfaces[18]) and is chemically inert and mechanically strong.[19]

The particles were produced by abrading a solid polymer sample of ETFE against a diamond lapping disc. Although the process of producing the ETFE particles in no way corresponds to the aggregation mechanism of actual protein particles, the morphology of the ETFE particles is remarkably similar to protein particles. Thus, the ETFE particles can serve as a surrogate to actual protein particles, with similar morphology and optical contrast. Like actual protein particle suspensions, but unlike PSL standards, the ETFE suspensions are polydisperse, with particles ranging in approximate sizes from greater than 50 μm down to less than 0.5 μm.

We produced polydisperse ETFE particles by first abrading ETFE against a diamond abrasive (45 μm nominal grit size, nickel bonded to a compliant backing) while submersed in an aqueous solution of 0.03 mol/L 2-[4-(2-hydroxyethyl)piperazin-1-yl]ethanesulfonic acid (HEPES) and 0.1% mass concentration sodium dodecyl sulfate (SDS) buffered to pH 6 (we intended to use pH 7.5, but inadvertently used a pH 6 buffer for the particle fabrication). At approximately 1 h intervals, the particle suspension was withdrawn by pipette from the well holding the abrasive disc. To prevent clogging of analytical instruments, large particles were filtered out by passing the suspension through a nylon screen with nominal 53 μm square openings. The nylon screen did not shed an appreciable number of particles if it was securely mounted, not folded or manipulated during the filtering process, and thoroughly rinsed with particle-free water prior to use. As harvested, the particle count was too high for direct measurement in some instruments. The suspension was diluted to the desired particle count with additional HEPES/SDS solution buffered to a pH of 7.5. Prior to use, the HEPES/SDS solution was filtered through a 0.45-μm PVDF syringe filter (Millex-HV; EMD Millipore, Billerica,

Massachusetts). (Certain commercial equipment, instruments, or materials are identified in this document. Such identification is not intended to imply recommendation or endorsement by the National Institute of Standards and Technology, nor is it intended to imply that the products identified are necessarily the best available for the purpose.) The large concentration of SDS proved necessary to promote dispersion of the highly hydrophobic ETFE particles: measurements on suspensions with an SDS concentration below 0.03% mass concentration had poor repeatability.

The suspension was packaged in perfluorinated alkoxy (PFA) screw-top vials with flat interior bottoms. PFA has several desirable attributes. First, PFA, with its low refractive index (1.34), does not produce thread debris of high optical contrast on repeated opening and closing of the vials. Second, the PFA vials have minimal leachates. Initial studies with glass screw-top vials revealed unacceptable quantities of debris created by friction between the screw top and the vial. Studies with polypropylene vials revealed that strong agitation (necessary to resuspend the ETFE particles) would produce long-lasting, vesicle-like droplets, likely as a result of combining SDS with organic leachates. These observations motivated the switch to the more expensive PFA vials.

Transfer of homogeneous aliquots of ETFE solution to a large number of vials is hampered by the fast settling of the ETFE particles relative to PSL beads. The ETFE particles were maintained in suspension in a 400 mL, open-top PFA jar by placing four stainless steel baffles around the periphery of the jar and then stirring at 200 revolutions per minute.[20] From this stirred jar, the suspension could be transferred by pipet into the PFA vials. Once in the vials, the suspension was further diluted by addition of the 0.03 mol/L HEPES, pH 7.5, 0.1% mass concentration SDS solution.

The threaded joint of the PFA vials can leak because of cold flow of the PFA over the course of several days. To prevent this problem, the vials were tightened after sitting overnight, and again after 7 days from the filling date. Rocking the lids back and forth while tightening also helped to promote a tight seal. Participants weighed the vials on receipt to ensure that the vials had not leaked during shipping; all vials were successfully shipped without leakage.

The vials were stored and shipped to participants at ambient temperature.

Characterization of the Particle Suspension

Variability of the Particle Concentration

On initial production, there are vial-to-vial variations in particle count because of irrepeatability of the dispensing and diluting process. After initial production, there are several potential mechanisms for further changes of the particle size distribution. As examples, agitation because of shipping or resuspension can potentially either break apart particles or cause abrasion of the PFA vials; sedimentation and natural convection can lead to entanglement of particles; and resealing the threaded closures can add abraded PFA particles.

To quantify vial-to-vial variations and possible changes in particle size distribution during storage, five vials were measured by light obscuration over a 3-month period corresponding to the period of data collection by the participants. Changes in particle size distribution were estimated from the changes observed for a single vial shipped from Maryland to California and back again. Separate experiments were conducted to repeatedly reseal three vials (which can lead to creation of thread debris), and measure the particle size distribution periodically by both light obscuration and flow imaging, for a total of 30 sealing cycles. The vial stability tests were conducted with multiple vials, opened at staggered time points, to reduce the effects of vial resealing on the stability test.

From the variations observed in these experiments, the standard uncertainty was determined for each effect, which is equivalent to the expected variations of any one vial from the mean of all vials at a confidence limit of 68% (i.e., equivalent to one standard deviation). The combined uncertainty u_c (i.e., the uncertainty attributed to all terms) was calculated by taking the square root of the sum of the squares of all uncertainty components. (The results of this analysis are given in the Supplementary Information as Table S1.) The value of u_c is an acceptable 8% for particle concentrations with a lower size limit of 5 μm or lower. For higher limits, u_c climbs to 19% at a lower limit of 25 μm. The larger value of u_c for a lower limit of 25 μm results at least in part from the low particle concentration in that size range, with $N \approx 80$ mL^{-1} (mL^{-1} is the unit symbol designating units of particles per milliliter). This low value increases the impact of small numbers of additional contaminants.

Although the stability of the ETFE particle suspension was sufficient for the purposes of this comparison, some drift in results were noted by both NIST and one participant. Part of this observed drift is likely because of thread debris, as discussed in section *Overview and Identification of Outliers*. One possible additional source of drift is microbial growth: despite the ability of SDS to denature proteins, bacteria have been observed to degrade SDS at concentrations in excess of the 0.1% mass concentration used here.[21,22] Subsequent to the data acquisition phase of the comparison, a stability test was initiated on ETFE particle suspensions of similar particle size distribution, but with the addition of 0.02% mass concentration of sodium azide and with greater care in filtration of the buffer. The stability of this second lot over 6.5 months was a factor of 1.9 better than the stability of the comparison lot over 3 months (data not shown).

Particle Morphology

We examined the particle morphology using both optical and electron microscopy. Examples of both types of images are shown in Figure 1. Optical images of the ETFE particles were acquired in suspension, using a flow imaging system with 10× magnification and a 100-μm thick flow cell.

Optical imaging of the ETFE particles is limited by the resolution of optical microscopy; scanning electron microscopy (SEM) has the potential of providing images with much higher resolution. However, the particles must be deposited on a substrate in such a way that the particles do not agglomerate on drying and must have the high SDS and HEPES concentration washed off. For SEM imaging, the particles were first captured on anodized alumina filters (Anodisc brand; GE Healthcare Bio-Sciences, Pittsburgh, Pennsylvania) with 0.2 μm diameter pores. Prior to use, the filters were first washed with water and then with a mixture of photoresist remover and ethanol. After oven drying, the filters were sputter coated on both sides with 25 nm of a Au/Pd alloy. The coated filter was placed on the glass-frit support of a vacuum flask, and 300 μL of water was pipetted

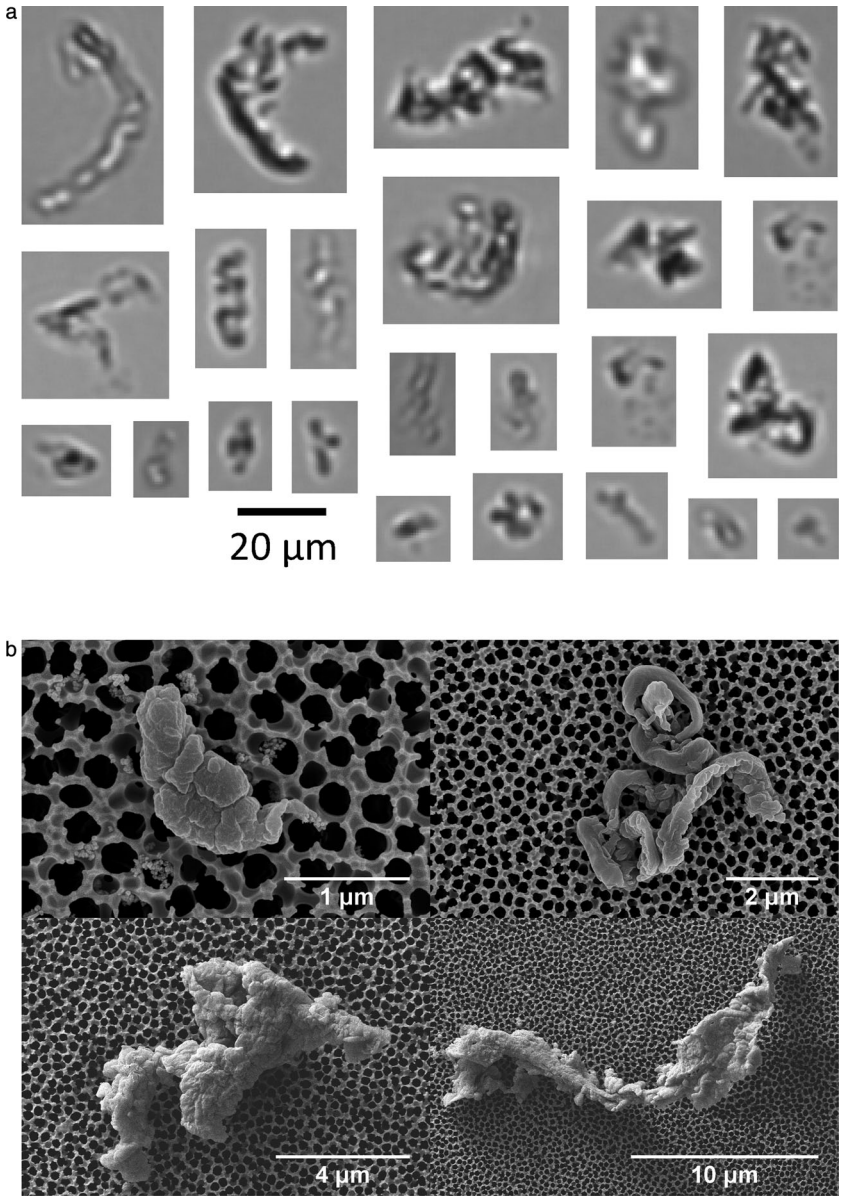

Figure 1. Example images of ETFE particles by (a) flow imaging, using 10× magnification, and (b) SEM of particles captured on a nanoporous alumina filter.

onto the top of the filter to form a nearly hemispherical "dome" on the hydrophobic Au/Pd film, whereas a slight partial vacuum (≈1.3 kPa, as determined by a vacuum manometer) was applied to the flask, sufficient to draw liquid through the filter at approximately 0.6 mL/min. A 100-µL sample of the ETFE suspension was slowly pipetted into the center of the dome; as the dome returned to an approximate volume of 300 µL, 100 µL of water was slowly pipetted into the top of the dome. This process was repeated until the desired particle count was achieved. The particles were then rinsed by 10 successive additions of 100 µL of water. After the rinse step, the vacuum was maintained to draw the water fully through the filter. Following drying of the filter in place, the filter was removed and a 25-nm top coat of Au/Pd film was sputter deposited. SEM images were obtained on a Zeiss scanning electron microscope at an electron energy of 5 keV, with both in-lens and conventional secondary electron detectors. Dispersive X-ray analysis conducted on the SEM confirmed that we were imaging fluorocarbon particles.

Inspection of the microscopic images shows them to be irregular and somewhat fibrous. We wished to characterize the average fraction of solid ETFE within the overall envelope of the particle, in anticipation that this packing fraction would help us understand differences in the particle counts obtained by different methods. The technique of quantitative phase microscopy[23,24] produces a phase map of the apparent optical phase difference $\phi(x, y)$, which is proportional to the difference in optical thickness between the particle and the matrix liquid:

$$\varphi(x,y) = \frac{2\pi\Delta n_{\mathrm{E}} z_{\mathrm{E}}}{\lambda_0}, \tag{1}$$

where Δn_E is the refractive index difference between solid ETFE and the matrix liquid, z_E is the total thickness of ETFE in the vertical z direction, x and y are lateral dimensions in the image plane, and λ_0 is the wavelength of light in vacuum. Integrating Eq. (1) over the whole area of the particle relates the integral of the optical phase difference over the whole particle area, Φ, to the total volume displaced by solid ETFE, V:

$$\Phi = \frac{2\pi\Delta n_E V}{\lambda_0}. \quad (2)$$

From the literature, the refractive index of ETFE, at the wavelength of 527 nm used here, is 1.400.[17] From measurements with a calibrated Abbe refractometer, the HEPES/SDS buffer has a refractive index of 1.337, giving $\Delta n_E = 0.063$ in Eqs. (1) and (2).

Published literature for objects with a thickness comparable to the width and length report that correcting phase values from the thin-object algorithm of Paganin and Nugent[23] by a factor of either two to five (varying with object size and using white light illumination)[24] or one (using highly coherent light).[25] In our implementation, we used partially coherent green light at a wavelength of 527 nm. To determine the correction factor, we suspended small glass beads in two liquids (one with negative Δn and one with positive Δn) and obtained a correction factor of 2.0 ± 0.1 (median and standard uncertainty of the median[26]) that was approximately independent of bead size (see Fig. S1, Supporting Information).

Two of the counting methods reported in this comparison, ESZ and RMM techniques, report equivalent diameters d_V that are equal to the diameter of a sphere with volume V:

$$V = (\pi/6)\, d_V^3. \quad (3)$$

Flow imaging reports an effective diameter, d_F, that is either an average of dimensional measurements across the optical image or the diameter of a circle with the same area as the imaged particle:

$$A = (\pi/4)\, d_F^2. \quad (4)$$

The final method, light obscuration, reports a diameter that is based on an angle integration of scattered light, which is not directly related to the physical particle dimensions.

To determine the relation between d_V and d_F for the ETFE particles, we obtained brightfield images on a number of ETFE particles in suspension in the matrix liquid (using Kohler illumination at a wavelength of 527 nm, with a 20× magnification, 0.40 numerical aperture objective). As the particles settled to the bottom of the counting chamber, the long axis of the particles was approximately normal to the optical axis. Thus, the particles were similar in orientation to particles that were aligned along the flow direction in the flow cell of a particle counter. We denote the effective diameter of aligned and randomly oriented particles as $d_{F,A}$ and $d_{F,R}$, respectively. Direct analysis of the brightfield images using ImageJ software[27] gave the projected area of each particle, and by Eq. (4), a value of $d_{F,A}$. Quantitative phase analysis of two images obtained at a focal plane difference of 2 μm gave the phase map $\phi(x, y)$, from which we obtained d_V by Eqs. 1–3. From an analysis of 80 particles ranging in diameter from 2 to 29 μm, we determined that the average ratio $d_V/d_{F,A}$ varied smoothly from a value of 0.90 ± 0.10 (mean and standard error of the mean for 13 particles) at 2 μm diameter to 0.51 ± 0.02 (mean and standard error of the mean for 10 particles) at 20 μm diameter. For randomly oriented particles, there is a small correction because of the difference between the average cross-sections of a randomly oriented particle and the cross-section of an aligned particle. Approximating the particles as prolate spheroids with aspect ratio $\eta \approx 0.6$ (see Table S2 in the Supplementary Information) gives a ratio[28] $d_{F,A}/d_{F,R} = \eta^{-1/6} = 1.08$ as a correction factor to convert $d_V/d_{F,A}$ to $d_V/d_{F,R}$.

Absolute Particle Concentration

For the purposes of the present interlaboratory comparison, we did not determine a particle size distribution traceable to the International System of Units. To do so requires careful development of techniques to size and count particles with minimal bias. On successful development of appropriate techniques, we plan to release this ETFE suspension as a reference material certified for particle size distribution and morphological properties such as the average aspect ratio.

Comparison Protocol

The testing of the ETFE particles was much more challenging to the participating laboratories than measurement of commercial PSL-bead count standards. The participants were not given the particle count or the particle size distribution, and the polydisperse nature of the sample made it hard to distinguish true particles from any contaminants or other source of spurious counts. In this regard, measurement of the ETFE was very similar to measurement of an actual biotherapeutic candidate or product. The protocol and data reporting template did not specify the type of instrumentation to be used for this, although the template did include columns already set up for the two most prevalent methods: flow imaging and light obscuration.

One parameter in which the ETFE differs substantially from PSL beads is its high density, which causes ETFE particles to sediment much faster than PSL beads of the same hydrodynamic radius. To mitigate this effect, guidance on methods to reduce sedimentation effects was distributed to the participants.

The high density of the ETFE, combined with the irregular morphology, can lead to entanglement of the ETFE particles following sedimentation. Prior experiments at NIST demonstrated that the best method to resuspend particles was to hold the vials horizontally and then shake vigorously for 20 s. This method resuspended particles much more effectively than either sonication or vortexing. The protocol (see the Supporting Information) gave instructions to the participants on this resuspension technique.

To maintain confidentiality, all data were submitted to a third-party data handling organization, which submitted anonymous data to NIST. Data was reported by the participants using a spreadsheet template. The template included columns for instrumentation type and settings, the particle concentrations for equivalent diameters equal to or greater than 1, 2, 5, 10, 15, 20, and 25 μm, and standard deviations of the obtained concentrations.

RESULTS AND DISCUSSION

Overview and Identification of Outliers

Of the 24 laboratories reporting data, data from 22 laboratories are fully reported here, along with half the data from one other laboratory. Complete records of all 24 data sets are available in the Supporting Information (round 1 data sets); data sets are identified by the laboratory code assigned by the data-handling organization. In some cases, laboratories reported data for multiple instruments of the same type (e.g., flow imaging microscopes) but different models; these reported values were treated as independent data sets.

Data from three laboratories were identified as outliers (laboratory codes B4893, B2899, and H2894; full data sets included in Supporting Information). For laboratory code B2899, the counts were consistently high for three different counting methods, indicating some contamination or failure of the transfer standard. In an effort to identify the cause of the discrepancy, an additional sample of ETFE (labeled as round 2 in the Supporting Information) was sent to this laboratory. The laboratory returned both the data reporting sheet and a detailed sheet of raw data. From the raw data, it became apparent that this participant acquired more replicates than almost all other participants and that the anomalies were greatest at large particle size and near the end of the sample volume. This pattern is consistent with contamination of the sample with thread debris. The magnitude of the effect is larger than included in the uncertainty budget for two reasons: the number of replicates was quite high, and the NIST experiments did not draw down the sample volume as rapidly as the B2899 experiments (as the sample volume decreases, a given amount of added thread debris will have a larger proportional effect). To mitigate the effects of thread debris on this data set, we included only the first set of three replicates obtained by B2899. On doing so, this data set was no longer an outlier.

For laboratory code H2894, counts were especially high at large diameter limits for flow imaging, but not for light obscuration. Inspection of the dates of data acquisition revealed that the flow imaging data were taken after a large volume of the sample was used for light obscuration data. On the basis of the pattern of discrepancies, which was similar to that observed with B2899, it is possible that the H2894 flow imaging data set was similarly affected by thread debris. Flow imaging data for H2894 was not included in the analysis below.

Finally, for laboratory code B4893, particle counts were consistently low for both flow imaging and light obscuration. Insufficient resuspension of the ETFE particles may have caused these low counts. Data for B4893 were not included in the analysis below. Additional observations about the various data sets and sources of discrepancies are discussed in the sections below.

The predominant methods used by the participants were light obscuration (19 data sets) and flow imaging (25 sets). Three laboratories also measured the suspension using ESZ instruments (commonly known as Coulter counters), and one laboratory reported data using resonance mass measurement. Figure 2 and Table 2 present the average of the cumulative particle concentration N (i.e., count per milliliter for particles greater than or equal to the indicated diameter) and the relative standard deviation among the laboratories for the 20 data sets, for these four particle counting methods.

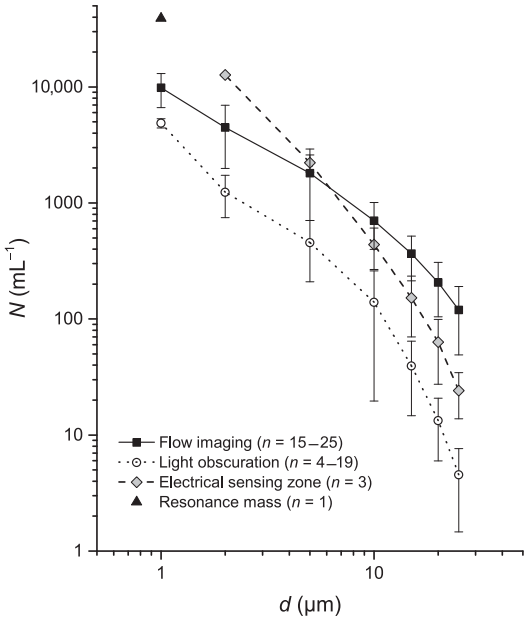

Figure 2. Unweighted means of the cumulative particle concentration N as a function of the lower diameter limit d for four particle counting methods. Error bars indicate standard deviations of the reported data sets, and the number of data sets in each average is reported in parenthesis.

As expected, the light obscuration values lie considerably lower in count than the flow imaging values. The cause of this reduced count is known to be because of the small refractive index difference between the particles and the matrix fluid, which leads to the light obscuration instruments reporting diameter values that are lower than observed by flow imaging.[10,29] For the ETFE particles used in this comparison, light obscuration undersizes the particles by approximately a factor of two, relative to flow imaging. This factor can be determined by finding the ratio of flow imaging diameter to light obscuration diameter for a fixed particle concentration.

Flow Imaging

The comparison data included data from multiple models of flow imaging systems manufactured by two companies (see Fig. 3). Participants obtained data using a wide range of system magnification (4× to 20×), flow cell depth (80–400 μm), and particle identification algorithms.

As a result of differences between instrument response, the RSD values for all of the combined flow imaging data sets ranged from 33% to 61%, as listed in Table 3. Selected data sets showed better RSD values. For instruments from manufacturer A, RSD values ranged from 21% to 36% (n = 18), even with flow cells of both 100 and 400 μm thickness and several magnifications. For instruments from manufacturer B, with 10× magnification, capture thresholds that selected both dark and light pixels, and 80 or 100 μm flow cell thickness (n = 4), RSD values ranged from 38% to 49%. We applied a two-tailed, unpaired T-test to ascertain the statistical significance of the apparent differences in counts obtained from these two restricted data sets. For diameter limits of 5 μm and larger, the t-test showed statistical significance at greater than 95% confidence (i.e., $p < 5\%$).

Table 2. Mean Cumulative Concentration *N*, Relative Standard Deviation RSD, and Number of Data Sets *n* for Four Measurement Techniques

	Flow Imaging			Light Obscuration			ESZ			RMM		
d (μm)	*N* (mL^{-1})	RSD (%)	*n*	*N* (mL^{-1})	RSD (%)	*n*	*N* (mL^{-1})	RSD (%)	*N*	*N* (mL^{-1})	RSD (%)	*n*
1	9858	33	15	4882	9	4	NA	NA	0	38,967	NA	1
2	4515	55	24	1241	40	19	12,700	NA	1	NA	NA	0
5	1822	60	25	457	54	18	2217	17	3	NA	NA	0
10	705	43	25	140	86	19	438	39	3	NA	NA	0
15	363	42	24	39	63	16	152	54	3	NA	NA	0
20	204	51	23	13	55	15	63	57	3	NA	NA	0
25	118	61	25	5	68	19	24	43	3	NA	NA	0

Refer to the text regarding adjustments to the data set.

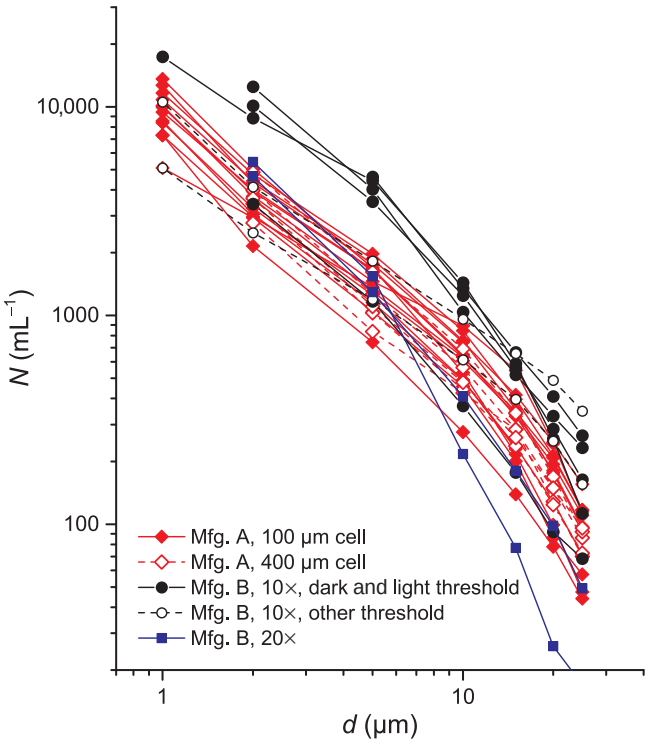

Figure 3. Flow imaging data for the cumulative particle concentration N as a function of the lower diameter limit *d*. Data obtained from manufacturer A instruments are red-filled diamonds and solid lines for 100 μm thick flow cells and red open diamonds and dashed lines for 400 μm thick flow cells. Data from manufacturer B instruments are black dots and solid lines for 10× magnification and known dark and light thresholds applied; black circles and dashed lines for 10× magnification and dark only or unknown thresholds; and blue squares and lines for 20× magnification. Each symbol reports the mean of multiple measurements obtained by the reporting laboratory for each data set; error bars are omitted for clarity, but repeatability values may be found in the Supporting Information.

For manufacturer B, many of the instruments had variable detection thresholds and user-specified focus. Referring to Figure 3 (open black circles), two data sets using manufacturer B instruments at 10× magnification and either dark threshold only or unidentified threshold had counts that were very close to those of manufacturer A results, whereas four of five data sets with both dark and light threshold settings gave counts significantly higher than manufacturer A instruments. This suggests that standardization of threshold settings may be useful in achieving better reproducibility between laboratories.

Two data sets using an instrument from Manufacturer B set up with 20× magnification gave counts for larger particles considerably lower than other data sets obtained using 10× magnification (blue symbols in Fig. 3). A possible reason for this discrepancy is that the short depth of field of the 20× objective, coupled with the irregular, low-contrast nature of the ETFE particles led to particles far from the focal plane not being detected.

Flow imaging instruments are capable of measuring a large number of morphological parameters for particles larger than the optical resolution of the system. The data reporting template included an option to report the average measured aspect ratio for the different size bins. The reported values agree quite well except for one outlier. Standard deviations for the different size ranges varied from 0.04 to 0.18 with the outlier included, or from 0.04 to 0.07 for all the data (see Table S2 in the Supplementary Information). No statistically significant difference was observed between results obtained with different manufacturer's instruments. The aspect ratio values (0.62 for particles larger than 10 μm) clearly indicate the nonspherical nature of the ETFE particles.

Two participants (A2813 and L2493) obtained data using robot-loaded flow imaging systems. The robotic systems have automated sample stirring, priming of the flow cell, and measurement of particles. At the beginning of the comparison, it was not clear whether the standard instrumentation software could accommodate the ETFE standards, given the tendency of the ETFE to sediment. In fact, these data sets showed excellent repeatability, with RSD varying from 2% to 9%. One other participant (W2481) submitted two sets of data obtained by loading two flow imaging systems from a continuously stirred, open syringe, obtaining data consistent with other data sets.

Comparison participants voiced concerns over sedimentation of the ETFE. Sedimentation velocity of a spherical body increases as the square of the diameter. Consequently, neglecting the impact of variations in geometry with particle size, a 25-μm particle would have a sedimentation velocity 2.8 times larger than a 15-μm particle. Examining how the deviations of outlier data sets varied with diameter showed no obvious patterns characteristic of errors that would scale as d^2.

The repeatability reported by each participating laboratory (RSD_i) was excellent for the full range of diameter limits reported (see Table S3 in the Supplementary Information).

 DOI 10.1002/jps.24287

Table 3. Flow Imaging Data for Cumulative Concentration N, Relative Standard Deviation RSD, and Number of Data Sets n, for Different Values of the Lower Diameter Limit d

	All Data			Manufacturer A, 100 µm Flow Cell			Manufacturer A, 400 µm Flow Cell			Manufacturer B, 10× Magnification, Dark, and Light Thresholds		
d (µm)	N (mL^{-1})	RSD (%)	n	N (mL^{-1})	RSD (%)	n	N (mL^{-1})	RSD (%)	n	N (mL^{-1})	RSD (%)	n
1	9858	33	15	9574	25	11	NA	NA	0	13,943	NA	1
2	4515	55	24	3707	22	12	3739	21	5	7794	44	4
5	1822	60	25	1457	24	12	1170	25	5	3260	39	5
10	705	43	25	616	28	12	520	21	5	1066	39	5
15	363	42	24	312	36	11	281	14	5	528	38	5
20	204	51	23	168	36	10	144	13	5	310	43	5
25	118	61	25	91	36	12	83	14	5	199	49	5

All participants achieved RSD_i values less than 33% for diameter limits of 10 µm or less, and 75% of participants (3rd quartile) had RSD_i values less than 26% for the full range of diameters.

Light Obscuration

Light obscuration was the second most common method reported by the comparison participants, with 19 data sets, after flow imaging. Because of the small refractive index difference between ETFE and the buffer solution ($\Delta n \approx 0.04$), light obscuration reported significantly fewer counts than flow imaging or ESZ techniques.[10,29] All of the data were obtained with instruments from two manufacturers, with several instrument models for each manufacturer. The instruments of one manufacturer had a lower diameter limit of 1.3 µm. Several participants reported the measured values for this limit, but data are not discussed further as this diameter limit was not one of the values on the data reporting template.

As seen in Figure 4 and Table 4, and confirmed by a two-tailed t-test, there were no statistically significant differences between data obtained from the two brands of instruments, over the full diameter range of the comparison. Plotting the data did reveal that data obtained with sensor heads designed for a 2 to 400-µm diameter particle size had significantly poorer reproducibility than sensor heads designed for particles smaller than 150 µm diameter. One participant (B2899, round 2) measured a second sample of ETFE on two instruments that had different sensor model numbers but the same nominal 2–400 µm diameter range. This single laboratory obtained counts that differed by over a factor of 10 (Supporting Information, round 2 data sheets, B2899-2). Further work should be carried out to understand why the reproducibility varies so much with relatively minor changes in sensor geometry.

One participant (B2188) obtained data at a flow rate of 1 mL/min and obtained particle concentrations that were anomalously low for large particle sizes. This effect is likely the result of ETFE sedimentation.

As noted in *Results and Discussion*, the light obscuration counters report an effective diameter that is approximately a factor of two smaller than the diameter reported from flow imaging. Thus, a lower apparent diameter limit of 25 µm for a light obscuration measurement corresponds to a physical diameter of approximately 50 µm. As the ETFE suspension was filtered through a nominal 53 µm screen in its preparation, the total count of particles with a 25-µm lower diameter limit is nearly zero.

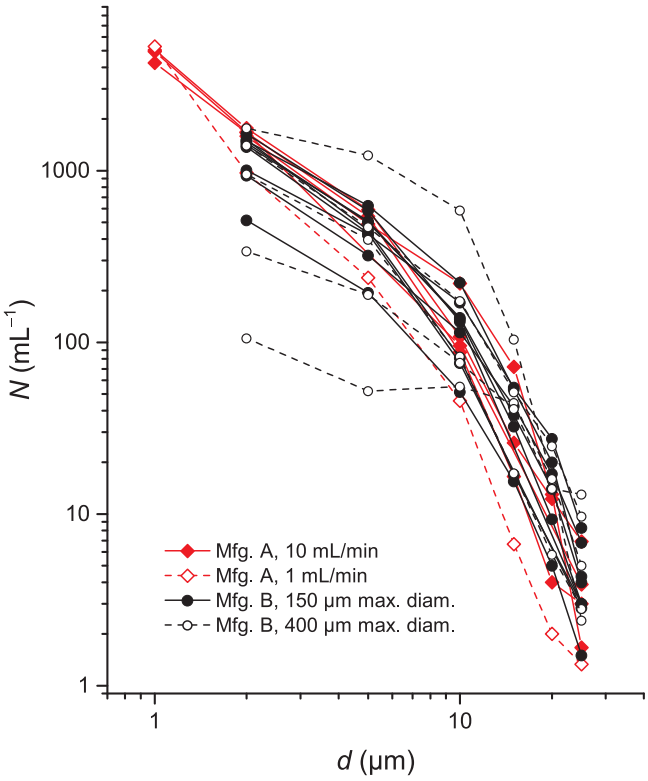

Figure 4. Light obscuration data for the cumulative particle concentration N as a function of the lower diameter limit d. Data obtained from manufacturer A instruments are red-closed diamonds and solid lines for data obtained at 10 mL/min, and red open diamonds and dashed lines for data obtained at 1 mL/min. Data from manufacturer B instruments are black dots and solid lines for instruments with a maximum diameter limit of 150 µm, and black circles and dashed lines for instruments with a maximum diameter of 400 µm. Each symbol reports the mean of multiple measurements obtained by the reporting laboratory for each data set; error bars are omitted for clarity, but repeatability values may be found in the Supporting Information.

The RSD values for the complete light obscuration data set range from 9% to 86%, as shown in Table 4. With data removed for instruments with a size range from 2 to 400 µm and from the one data set obtained at 1 mL/min, the RSD values are 9% at a lower diameter limit of 1 µm, rise to 26% at 5 µm, reach a peak of 54% for a lower diameter limit of 20 µm, and then

Table 4. Light Obscuration Data for Cumulative Concentration N, Relative Standard Deviation RSD Between Laboratories, and Number of Data Sets n, for Different Values of the Lower Diameter Limit d

	All Data			Sensor Heads for $d \leq$ 200 µm; Flow Rate (10–25 mL/min)			Sensor Heads for 2 µm $\leq d \leq$ 400 µm Sensor Heads		
d (µm)	N (mL^{-1})	RSD (%)	n	N (mL^{-1})	RSD (%)	n	N (mL^{-1})	RSD (%)	n
1	4882	9	4	4747	9	3	NA	NA	0
2	1241	40	19	1387	26	13	913	76	5
5	457	54	18	472	26	12	467	98	5
10	140	86	19	126	42	13	195	115	5
15	39	63	16	37	52	10	52	62	5
20	13	55	15	14	54	9	15	44	5
25	5	68%	19	4	52%	13	7	70%	5

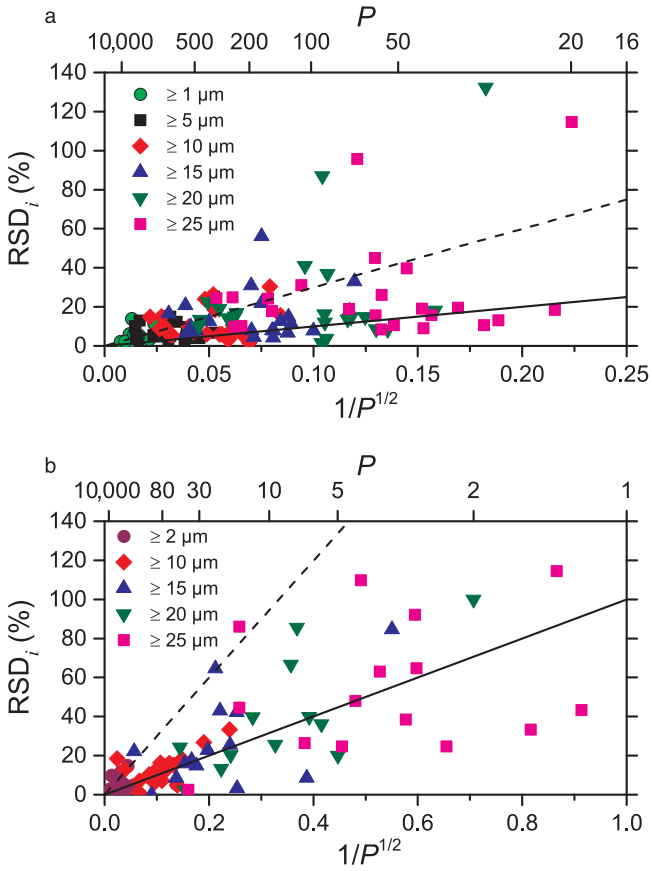

Figure 5. RSD$_i$ values versus 1/P$^{1/2}$ for both flow imaging (a) and light obscuration (b) data, where P is the number of particles measured per replicate. The solid line represents the expected RSD$_i$ values because of counting fluctuations alone, and the dashed line represents the upper bound for the contribution of counting fluctuations to RSD$_i$ at $p < 5\%$, for three replicates.

decline slightly at a diameter limit of 25 µm, in spite of the very small concentration detected.

The low-residual standard deviations for small diameter values appear to be counterintuitive, as light obscuration counters are known to have sensitivity to the optical properties of particles for diameters below approximately 10 µm (which is one justification why 10 µm is specified as the lower diameter limit in pharmacopeial methods[30]), which leads to inaccurate counts even for particles of high optical contrast. For transparent particles with low optical contrast, such as protein or ETFE particles, light obscuration has poor accuracy for all diameter limits (see Fig. S2 in the Supporting Information). Note, however, that the RSD between data sets is not a measure of the accuracy of the reported counts, but is instead a measure of the reproducibility of counts among similar instruments. The smaller RSD values at small diameter limits may occur because small particles scatter light over a broader angle than large particles; the instrument response may be less sensitive to details of aperture size and focus and alignment of the beam and flow cell.

The good agreement between laboratories for a lower diameter limit down to 1 µm demonstrates that light obscuration measurements can provide a repeatable, but not accurate, measure of particle concentration down to sizes much smaller than the 10-µm lower limit of pharmacopeial methods for samples of fixed optical contrast and morphology.[30]

The repeatability achieved by individual participants using light obscuration (see Table S4 in the Supplementary Information) appears to be significantly worse than that achieved with flow imaging, especially at large diameter limits. However, the poor repeatability in this case is partly because of undersizing of particles by light obscuration and the correspondingly low values of N at diameter limits of 15 µm and greater. At diameter limits of 10 µm or smaller, which corresponds to an equivalent physical diameter limit of approximately 20 µm or smaller, RSD$_i$ values for light obscuration are less than 16% for 75% of participants.

Statistical Variations of Light Obscuration and Flow Imaging Data

The particle size distribution of the ETFE suspension was constrained by several factors. First, to provide a realistic simulation of protein particles, the particle size distribution should rapidly decrease with increasing values of diameter. Second, for some light obscuration instruments commonly used in the pharmaceutical industry, an error of ≥10% occurs for particle concentrations of 10,000 mL^{-1} or higher, because of multiple particles traversing the sensing zone simultaneously. Finally, the number of particles with $d > 100$ µm must be nearly zero to avoid clogging instrument inlets. A significant consequence of keeping the overall concentration below 10,000 mL^{-1} combined with the rapid reduction in $N(d)$ as d increases is that significant errors can be introduced by the limited number of particle counts, especially for size bins of $d \geq 15$ µm and larger.

The RSD$_i$ because of counting statistics is $1/P^{1/2}$, where P is the number of particles measured per replicate. Figure 5 shows RSD$_i$ values versus $1/P^{1/2}$ for both flow imaging (Fig. 5a)

 DOI 10.1002/jps.24287

and light obscuration (Fig. 5b) data. Values for P were calculated from the reported measurement volumes and by assuming sampling efficiencies of 100% for light obscuration, 85% for flow imaging instruments from manufacturer A, and 35% for flow imaging instruments from manufacturer B. The solid line represents the expected mean RSD_i values because of counting fluctuations, $(100\%)/P^{1/2}$. The dashed line represents the upper bound for the contribution to RSD_i from counting fluctuations, at a confidence level of $p < 5\%$ and three replicate measurements (i.e., F-distribution evaluated at 2 and infinite degrees of freedom, at a confidence level of 5%). Data have only a 5% likelihood of appearing above this line because of counting fluctuations alone.

For the flow imaging data set, the RSD_i values are tightly distributed for $d \geq 1$ μm through $d \geq 10$ μm data sets. The relative standard error of the mean of $N(d)$ is obtained by dividing RSD_i by the square root of the number of replicates; thus, if counting fluctuations contribute less than 30% to the RSD_i, relative SEM values of 17% are achievable with three replicates. The data sets for $d \geq 20$ μm and $d \geq 25$ μm illustrate that most of the participants achieved RSD_i values at this level for even the largest particle bins. There are two clear outliers well in excess of counting errors for each of these bins, and several points with RSD_i values near the $p < 5\%$ line.

For light obscuration, the undersizing of particles combined with the steep drop in the particle size distribution led to small numbers of particles detected. As a result, identification of laboratories with poor repeatability is difficult, but the comparison has sufficiently low counting uncertainties to enable reasonable comparison (i.e., relative SEM < 17%) of average $N(d)$ values for $d \geq 15$ μm bin and smaller.

Considering future formulations of particle suspensions, a fourfold increase in $N(d)$ for $d \geq 20$ μm and $d \geq 25$ μm would reduce the statistical uncertainty sufficiently to achieve a relative SEM < 20% for light obscuration at all size bins and a more unambiguous identification of poor repeatability for flow imaging in size bins of 20 μm and larger.

Resonant Mass Measurement

One participant reported data using the RMM technique, converting particle mass into an effective diameter using literature values for the ETFE density (≈1700 kg/m^3).[19] Because the ETFE density differs widely from the buffer solution (unlike protein particles in solution), this measurement is not a stringent test of RMM, and the NIST organizers did not anticipate that a test of the particles by RMM would have particular value. However, on considering the data, measurement of ETFE by both RMM and flow imaging may provide a very useful cross-check of flow imaging. The discrepancy between the RMM and flow imaging at the lowest diameter limit (1 μm) may be a consequence of the reduced visibility of low-contrast particles in flow imaging systems. Further pursuit of this approach may provide a method of validating flow imaging systems near the lower diameter limit of these instruments. One difficulty in the interpretation of the RMM data is that the reported diameter is equal to the diameter of a compact ETFE sphere, which differs from the diameter derived from the projected area by flow microscopy. A challenge in performing RMM on the circulated ETFE suspension is that the particle concentration is too low to give RMM counts with low statistical uncertainty for the small sample volumes typically used for RMM. The value of $N(d = 2$ μm) reported in Table 2 for RMM is equivalent to approximately four particles per replicate.

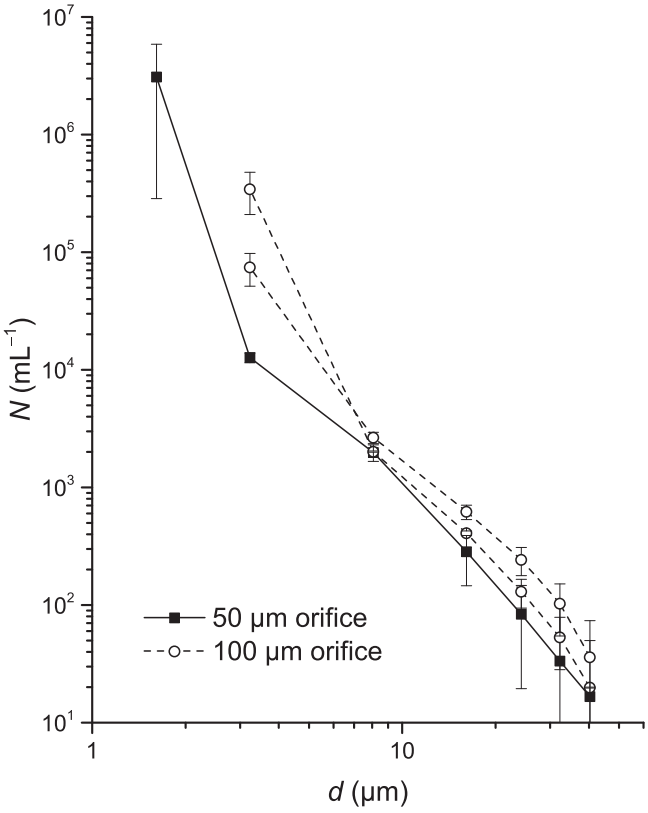

Figure 6. Electrical sensing zone data for the cumulative particle concentration N as a function of the lower diameter limit d, for two different orifice sizes. The arrow denotes possible data anomalies. Error bars indicate the standard deviation of the repeat measurements obtained by the reporting laboratory for each data set.

Electrical Sensing Zone

Two participants reported data using the ESZ technique. A sharp, likely anomalous increase in apparent particle count was observed at diameters near the lower limit of the ESZ instruments, as shown in Figure 6 and Table 5. The lower limit of the ESZ measurements depends on the size of the orifice installed in the instrument, and the anomalous increase shifts with a change in orifice. Similar increases in particle counts have been observed with polydisperse suspensions of actual protein particles.[15] Until the cause of the anomalous data can be ascertained, use of the ETFE suspension for ESZ instruments may be of limited value.

Electrical sensing zone instruments report diameters based on the displaced volume of the particle; in contrast, flow imaging reports a diameter based on the projected area. For the irregular, convoluted morphologies of the ETFE particles, the volume-based diameter can be substantially smaller than the area-based diameter. We attempted to correct this bias using the ratio of these diameters obtained from quantitative phase microscopy, as described in section *Particle Morphology*. The corrected ESZ results, for either aligned or randomly oriented particles, agree well with the flow imaging results for a lower diameter limit of 15 μm or larger, as seen in Figure 7. The method of section *Particle Morphology* leads to an apparent

Table 5. Electrical Sensing Zone Data for Different Values of the Lower Diameter Limit d Reported by the Participants (Equivalent to d_V in Eq. (3), and the Scaled, Area-Based Diameters for Aligned and Randomly Oriented Particles, $d_{F,A}$ and $d_{F,R}$, Obtained by the Method Discussed in Section *Particle Morphology*

			All Data Sets, Anomalous Data Removed			Data Taken with 50 µm Orifice			Data Taken with 100 µm Orifice		
d (µm)	$d_{F,A}$ (µm)	$d_{F,R}$ (µm)	N (mL^{-1})	RSD (%)	n	N (mL^{-1})	RSD (%)	n	N (mL^{-1})	RSD (%)	n
1	1.63	1.50	NA	NA	0	NA	NA	0	3,081,067	NA	1
2	3.26	3.00	12,700	NA	1	209,024	91	2	12,700	NA	1
5	8.16	7.49	2217	17	3	2334	19	2	1983	NA	1
10	16.3	15.0	438	39	3	515	29	2	283	NA	1
15	24.5	22.5	152	54	3	187	43	2	83	NA	1
20	32.6	30.0	63	57	3	78	45	2	33	NA	1
25	40.8	37.4	24	43	3	28	41	2	17	NA	1

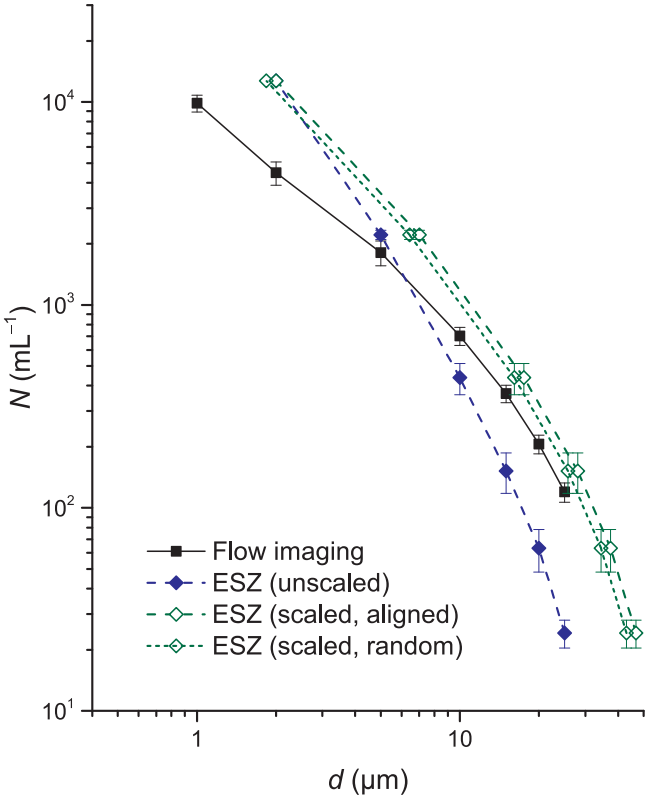

Figure 7. Electrical sensing zone data for N compared with flow imaging data, with and without diameter scaling of the ESZ diameters. Scaling is shown for particles that are randomly aligned (open diamond symbols, dashed lines) and aligned with the flow field (open diamond symbols, dotted lines). For flow imaging, error bars indicate standard error of the mean for the values reported by multiple laboratories. For ESZ, error bars indicate the standard error of the mean of the two data sets reported for a 100-µm orifice. At $d = 2$ µm, the ESZ data point indicates only the results of one laboratory with a 50-µm orifice.

overcorrection, possibly because the QPI measurements were performed on particles that were stationary on a glass slide. The method of section *Particle Morphology* assumes that the particle depth is equal to the particle width, but in fact the particles likely settle to the most gravitationally stable position, in which the particle has minimum thickness in the z direction. This settling effect will give a value of $d_V/d_{F,R}$ that is too low. At diameter limits between 1 and 5 µm, the correction increases the discrepancy between the ESZ results and the flow imaging values.

Because both RMM and ESZ instruments report an effective diameter based on the displaced volume, it is possible in theory to compare the results of these two types of instruments directly. In the present comparison, however, there is not sufficient overlap of the two data sets to allow a comparison. The one participant reporting RMM results includes data up to a lower diameter limit of 2 µm, but for this bin only two particles were detected for all three replicates combined, leading to a very high uncertainty in the particle concentration at this size. The ESZ data extend down to 1 µm, but the data for diameter limit of 1 µm are in the anomalous region. We encourage a future comparison between RMM and ESZ in the region of overlap

CONCLUSIONS

The combined data sets of this comparison provide a well-controlled and extensive data set to study discrepancies between the different counting methods. The discrepancies in particle counts of the ETFE suspension by the different measuring methods (a factor of 10 times in the worst cases) were comparable to the discrepancies seen for particles in actual protein solutions.

Selected subsets of the comparison data showed good reproducibility, comparable with the uncertainty of the ETFE suspension. In particular, for light obscuration measurements at a lower diameter limit of 5 µm, the RSD values were approximately 25%, and for flow imaging instruments of a single manufacturer, with fixed instrument series, RSD values were approximately 30% for all diameter limits. These values illustrate that for controlled instrument parameters, good reproducibility of particle counts can be obtained through a broad section of the biopharmaceutical industry, device and equipment manufacturers, and academic and government laboratories.

Better agreement between the different methods, or between instruments of different settings or manufacturer, will be the next challenge. Our partially successful attempt at adjusting the ESZ reported diameter to match an area-based diameter is an example of the bias correction methods that need to be developed.

Results of the comparison also provide useful information for the development of ETFE suspensions as a reference material.

The ETFE suspension proved generally useful as a tool to ascertain instrument performance, with the exception of ESZ instruments near the lower limit of the installed orifice. Increasing the particle concentration for particle diameters greater than 15 μm would increase the number of particles measured in the larger size bins, giving measurement results with less variability and reducing the effects of thread debris. The presence of data sets with very low values suggests that the instructions on resuspension of the sample were not clear enough. Sedimentation of the particles may have been a contributing factor as well; we are working with collaborators to mitigate this problem by adding viscosity modifiers to the ETFE suspension. It will also be useful to reinforce in the instructions that resuspension and stirring sample prior to use is necessary. The good success with robotic and continuously stirred samples demonstrated that the ETFE suspension is compatible with advanced sample handling instrumentation.

ACKNOWLEDGMENTS

We thank all the participating laboratories for supplying data for this study. We thank Charles Ellis of the National Association of Proficiency Testing for data handling services. Our SEM measurements were obtained at the NIST Center for Nanoscale Science and Technology, and we thank Kerry Siebein for help with these measurements.

REFERENCES

1. Carpenter JF, Randolph TW, Jiskoot W, Crommelin DJA, Middaugh CR, Winter G, Fan Y-X, Kirshner S, Verthelyi D, Kozlowski S, Clouse KA, Swann PG, Rosenberg A, Cherney B. 2009. Overlooking subvisible particles in therapeutic protein products: Gaps that may compromise product quality. J Pharm Sci 98:1201–1205.

2. Singh SK, Afonina N, Awwad M, Bechtold-Peters K, Blue JT, Chou D, Cromwell M, Krause H-J, Mahler H-C, Meyer BK, Narhi L, Nesta DP, Spitznagel T. 2010. An industry perspective on the monitoring of subvisible particles as a quality attribute for protein therapeutics. J Pharm Sci 99:3302–3321.

3. Joubert MK, Luo Q, Nashed-Samuel Y, Wypych J, Narhi LO. 2011. Classification and characterization of therapeutic antibody aggregates. J Biol Chem 286:25118–25133.

4. Bee JS, Chiu D, Sawicki S, Stevenson JL, Chatterjee K, Freund E, Carpenter JF, Randolph TW. 2009. Monoclonal antibody interactions with micro- and nanoparticles: Adsorption, aggregation, and accelerated stress studies. J Pharm Sci 98:3218–3238.

5. Bee JS, Randolph TW, Carpenter JF, Bishop SM, Dimitrova MN. 2011. Effects of surfaces and leachables on the stability of biopharmaceuticals. J Pharm Sci 100:4158–4170.

6. Tyagi AK, Randolph TW, Dong A, Maloney KM, Hitscherich C Jr, Carpenter JF. 2009. IgG particle formation during filling pump operation: A case study of heterogeneous nucleation on stainless steel nanoparticles. J Pharm Sci 98:94–104.

7. Nayak A, Colandene J, Bradford V, Perkins M. 2011. Characterization of subvisible particle formation during the filling pump operation of a monoclonal antibody solution. J Pharm Sci 100:4198–4204.

8. Zölls S, Tantipolphan R, Wiggenhorn M, Winter G, Jiskoot W, Friess W, Hawe A. 2011. Particles in therapeutic protein formulations, part 1: Overview of analytical methods. J Pharm Sci 101:914–935.

9. Ripple DC, Dimitrova MN. 2012. Protein particles: What we know and what we do not know. J Pharm Sci 101:3568–3579.

10. Zölls S, Gregoritza M, Tantipolphan R, Wiggenhorn M, Winter G, Friess W, Hawe A. 2013. How subvisible particles become invisible—Relevance of the refractive index for protein particle analysis. J Pharm Sci 102:1434–1446.

11. Huang C-T, Sharma D, Oma P, Krishnamurthy R. 2009. Quantitation of protein particles in parenteral solutions using micro-flow imaging. J Pharm Sci 98:3058–3071.

12. Sharma DK, King D, Oma P, Merchant C. 2010. Micro-flow imaging: Flow microscopy applied to sub-visible particulate analysis in protein formulations. AAPS J 12:455–464.

13. Narhi LO, Jiang Y, Cao S, Benedek K, Shnek D. 2009. A critical review of analytical methods for subvisible and visible particles. Curr Pharm Biotechnol 10:373–81.

14. Demeule B, Messick S, Shire SJ, Liu J. 2010. Characterization of particles in protein solutions: Reaching the limits of current technologies. AAPS J 12:708–715.

15. Barnard JG, Rhyner MN, Carpenter JF. 2012. Critical evaluation and guidance for using the coulter method for counting subvisible particles in protein solutions. J Pharm Sci 101:140–153.

16. Burg TP, Godin M, Shen W, Carlson G, Foster JS, Babcock K, Manalis SR. 2007. Weighing of biomolecules, single cells, and single nanoparticles in fluid. Nature 446:1066–1069.

17. French RH, Rodríguez-Parada JM, Yang MK, Derryberry RA, Lemon MF, Brown MJ, Haeger CR, Samuels SL, Romano EC, Richardson RE. 2009. Optical properties of materials for concentrator photovoltaic systems. In Proc 34th IEEE Photovoltaic Specialists Conference (PVSC), Philadelphia, Pennsylvania, June 7-12. pp. 394–399.

18. Vörös J. 2004. The density and refractive index of adsorbing protein layers. Biophys J 87:553–561.

19. DuPont™ Tefzel® fluoropolymer resin. Properties handbook. Accessed November 19, 2014, at: http://www2.dupont.com/Teflon_Industrial/en_US/assets/downloads/h96518.pdf.

20. Myers KJ, Reeder MF, Fasano JB. 2002. Optimize mixing by using the proper baffles. Chem Eng Prog 98:42–47.

21. Chaturvedi V, Kumar A. 2010. Isolation of sodium dodecyl sulfate degrading strains from a detergent polluted pond situated in Varanasi city, India. J Cell Molec Bio 8:103–1110.

22. Louvado A, Coehlo FJRC, Domingues P, Santos AL, Gomes NCM, Almeida A, Cunha A. 2012. Isolation of surfactant-resistant pseudomonads from the estuarine surface microlayer. J Microbiol Biotechnol 22:283–291.

23. Paganin D, Nugent KA. 1998. Noninterferometric phase imaging with partially coherent light. Phys Rev Lett 80:2586–2589.

24. Bellair CJ, Curl CL, Allman BE, Harris PJ, Roberts A, Delbridge LMD, Nugent KA. 2004. Quantitative phase amplitude microscopy IV: imaging thick specimens. J Microscopy 214:62–69.

25. Frank J, Matrisch J, Horstmann J, Altmeyer S, Wernicke G. 2011. Refractive index determination of transparent samples by noniterative phase retrieval. Appl Opt 50:427–433.

26. Muller JW. 2000. Possible advantages of a robust evaluation of comparisons. J Res Natl Inst Stand Technol 105:551–555.

27. Rasband WS. 1997–2012. ImageJ, U. S. National Institutes of Health, Bethesda, Maryland. Accessed November 19, 2014, at: http://imagej.nih.gov/ij/.

28. Jennings BR, Parslow K. 1988. Particle size measurement: The equivalent spherical diameter. Proc Royal Soc London Series A 419:137–149.

29. Knollenberg RG, Gallant RC. 1990. Refractive index effects on particle size measurement in liquid media by optical extinction. In Proc International Conference on Particle Detection pp 154–182.

30. US Pharmacopeia. 2012. USP/NF General Chapter <788>. Particulate matter in injections. In US Pharmacopeia, National Formulary, USP31-NF-26. Rockville, Maryland: USP.